

Analysis of scattered higher dimensional data using generalized Fourier interpolation

K. Gellerstedt ^{*a} and J. Sjölin^{†a}

^a*Stockholm University, Department of Physics*

March 1, 2022

Abstract

A method based on orthogonal function series interpolation of the square root probability density to analyze higher dimensional scattered data is presented. The method is targeted for the use-case when the model and/or data are available only as discrete events. While fast and efficient algorithms are well known for pseudo-spectral (grid node based) methods, this work focuses on a spectral (non grid based) approach. A typical application is the extraction of physics model parameters from events detected in high energy particle collisions. Several examples are provided and the performance is compared to existing conventional procedures. In some cases the method can be shown to behave as an optimal observable of the data, exemplified by the ability to approach the Cramer-Rao bound.

Keywords: Density estimation, Fourier series, optimal observable

^{*}karl.gellerstedt@fysik.su.se

[†]sjolin@fysik.su.se

d	l	Full tensor	Sparse tensor
2	2	9	6
2	10	121	66
10	2	59k	66
10	10	$2.5 \cdot 10^{10}$	185k
20	2	$3.5 \cdot 10^9$	231
20	5	$3.6 \cdot 10^{15}$	53130

Table 1: Number of terms for full and monomial sparse tensors.

1 Introduction

An important step in data analysis is to estimate the probability density¹ of the model and the data. In many cases, e.g. high energy collider physics, the model is of such complexity that it can only be made available as Monte Carlo simulated events² and the complete density can only be interpolated from the events. In low dimensions a fast and effective way to estimate the density is to create a histogram of the events. Another more analytical approach is to approximate the density with an orthogonal function series (generalized Fourier series), for an overview see e.g. Ref. [1]. Unfortunately, both these methods encounter problems as soon as the dimensionality increases.

Any attempt to perform analysis in high d -dimensional spaces ($d \geq O(10)$) must be able to cope with the so called “curse of dimensionality”. One way to see this is to construct a d -dimensional space as a tensor product of 1-dimensional spaces of orthogonal functions $\phi_k(x)$ of degree k . For two dimensions, labeled x and y , with eigenfunctions up to second degree, the full tensor becomes

$$f(x, y) = a_0\phi_0(x)\phi_0(y) + a_1\phi_1(x)\phi_0(y) + a_2\phi_0(x)\phi_1(y) + a_3\phi_1(x)\phi_1(y) + a_4\phi_2(x)\phi_0(y) \\ + a_5\phi_0(x)\phi_2(y) + a_6\phi_2(x)\phi_1(y) + a_7\phi_1(x)\phi_2(y) + a_8\phi_2(x)\phi_2(y).$$

The number of coefficients a_u and eigenvectors needed will scale exponentially as $(\max(k) + 1)^d$ and quickly become intractable. A way to postpone the exponential growth is to first realize that the terms in the series contain products of basis functions with a total degree much larger than practically needed. Hence limiting the maximal order l of the tensor will postpone the disaster and lead to a scaling of the type $\binom{d+l}{l}$ which scales as $O(d^l/l!)$ for large d and fixed l , i.e. polynomial instead of exponential growth with respect to the number of dimensions, see Table 1. Using this *monomial basis*, as an approximation of the full tensor, is common practice in e.g. computational economics [2], and it will be applied throughout this work unless explicitly stated. However, an important difference is that this work uses a spectral instead of the common pseudo-spectral approach. This means that the data points are not restricted to be on the grid defined by the roots of the basis function with the highest degree.

A fundamental property of a probability density is that it is strictly positive or zero. When approximating the density with a truncated orthogonal function series this is no longer guaranteed. A beautiful solution to assert the non-negative property is to require that the density is equal to the square of a real valued Fourier amplitude. As will be shown this requirement also has the beneficial side effect that the measured Fourier coefficients become uncorrelated. The square root operation required by the method is solved in the sections below by iteratively reweighting the Fourier series into the series representing the square root of the density.

¹Throughout this text the term *density* will be considered synonymous with *probability density*.

²The term *event* denotes a unit of a statistical sample.

2 Background

2.1 Basics

The starting point for deriving the method is the fact that an orthogonal function series can be used for interpolation of sampled data. The outlined method can in principle use any orthogonal function series as long as the data is within its domain and the norm allows for sampling³. The selected orthogonal series should preferably be chosen to match the properties of the approximated density to allow for a minimal required set of eigenfunctions, e.g. spherical harmonics in case of spherical symmetry. The derivation begins with assuming a true one dimensional density function $p(x)$ which is defined on a bounded interval on the real line. This means that $p(x)$ is locally integrable and from this also follows that $p(x) \in L^1 \cap L^2$. Let $P(x) = np(x)$ be the scaled density where n is the expected size such that

$$\int P(x)dx = \int np(x)dx = n.$$

Since $P(x) \in L^2$ it means that $P(x)$ can be represented as an orthonormal real valued function series

$$P(x) = \sum_{k=0}^{\infty} \alpha_k \phi_k(x).$$

A natural observable for the true Fourier coefficients α_k given N events from the density $P(x)$, is

$$\begin{aligned} \alpha_k &= \langle P(x), \phi_k(x) \rangle = \int_V P(x) \phi_k(x) dx = n \int_V p(x) \phi_k(x) dx = n \langle \phi_k(x) \rangle_{p(x)} \simeq \frac{n}{N} \sum_{x_i \sim p(x)}^N \phi_k(x_i) \\ &= \{N \simeq n \text{ when } N \text{ is large}\} \simeq \sum_{x_i \sim p(x)}^N \phi_k(x_i) = a_k. \end{aligned} \quad (1)$$

The expectation operator and the sum use a notation that makes the underlying probability distribution explicit. From the last sum it is clear that events from data or Monte Carlo simulations which are drawn from the distribution $p(x)$ directly can be used for an efficient projection of $p(x)$ onto the normalized eigenvector $\phi_k(x)$. The extension to weighted events is straight forward, just substitute $\phi_k(x_i) \rightarrow \phi_k(x_i)w_i$.

2.2 Filtering

The observable for the coefficients α_k built from sampled projections in Eq. (1) can be turned into an optimal observable for $P(x)$ by the use of optimal filtering. An optimally filtered orthogonal series⁴

$$P(x, \lambda(N), \mathbf{a}) = \sum_k^{\infty} \lambda_k(N) a_k \phi_k(x),$$

can be found [3] by minimizing the mean integrated squared error (MISE)

$$\min_{\lambda(N)} \int_V |P(x) - P(x, \lambda(N), \mathbf{a})|^2 dx.$$

The solution for the optimal filter coefficients is

$$\lambda_k(N) = \frac{\alpha_k^2}{\alpha_k^2 + N \text{var}(\phi_k(x))}.$$

³An example which does not work is first kind Chebychev polynomials which have a norm with singularities at the boundaries.

⁴Throughout this text, \mathbf{a} will denote a vector or vector valued function, a_i will denote the i :th element of \mathbf{a} while \mathbf{a}_n is the n :th instance of \mathbf{a} .

Unfortunately in practice these coefficients are not easily obtained, since both $p(x)$ and its true coefficients α_k are unknown. Instead for large N a much more useful near optimal solution is given by $\lambda_k(N) = 1$ for $k \leq M(N)$ and $\lambda_k(N) = 0$ for $k > M(N)$, where $M(N)$ is a tuned highest order truncation. This means that $P(x, \lambda(N), a)$ is replaced by

$$P(x, M, \mathbf{a}) = \sum_k^{M(N)} a_k \phi_k(x),$$

The extension to higher dimensions is done by forming a tensor product of one dimensional orthogonal series for each dimension.

3 The SFI method

The construction of the generalized Fourier series in higher dimensions outlined below will be referred to as Sparse Fourier Interpolation (SFI). The key components of SFI are the sparse monomial basis, to postpone the curse of dimensionality, and a squared Fourier amplitude mapping asserting a strictly positive approximation. The function $P(x)$ is assumed to be approximated by a tensor build from products of truncated one-dimensional orthonormal eigenfunctions $\phi_k(x)$ of degree k .

3.1 Basis construction

Two orthonormal sets have been found to be useful for general purposes:

$$\phi_k(x) = \sqrt{\frac{2k+1}{2}} P_k(x)$$

where $P_k(x)$ are the Legendre functions on the interval -1 to 1, and

$$\begin{aligned} \phi_k(x) &= \sqrt{2} \cos(k\pi x), k > 0, \\ \phi_0(x) &= 1, \end{aligned} \tag{2}$$

which are the orthonormal finite Fourier cosine functions on the interval 0 to 1⁵. In the following examples the finite cosine functions are mainly used since they in these cases seem to work better. The density is expressed in the Fourier coefficient vector \mathbf{a} as:

$$P(\mathbf{x}, \mathbf{a}) \simeq \sum_u^{M(N)} a_u \phi_j(x_1) \phi_k(x_2) \dots = \sum_u^{M(N)} a_u \phi_u(\mathbf{x}),$$

where $M(N)$ is the number of eigenvectors when $j + k + \dots \leq l$, and l is the highest sum of degrees present in $P(\mathbf{x}, \mathbf{a})$.

3.2 A positive probability density – the square root and diagonalization

Even if $P(\mathbf{x})$ is originally non-negative, there is no such guarantee for $P(\mathbf{x}, \mathbf{a})$ after the truncation of the Fourier series. To assert a non-negative density, the method assumes that $P(\mathbf{x})$ can be written as

$$P(\mathbf{x}) = A^2(\mathbf{x}) \simeq A^2(\mathbf{x}, \mathbf{b})$$

and the problem is recasted as finding the coefficients in the Fourier series $A(\mathbf{x}, \mathbf{b})$, and A is not required to be positive. To differentiate between the previous linear SFI transform we refer to the method of finding A as the square root transform, or simply SFI. Since $A(\mathbf{x}, \mathbf{b})$ appears squared, Plancherel's theorem can be applied to $P(\mathbf{x})$

$$n = \int_V P(\mathbf{x}) d\mathbf{x} \simeq \int_V A^2(\mathbf{x}, \mathbf{b}) d\mathbf{x} = \sum_u |b_u|^2.$$

⁵In the code implementation the interval $[0, 1]$ is mapped to $[-1, 1]$ to simplify the use of the Legendre eigenfunctions.

It turns out that the noise modelling in this case is greatly simplified since the covariance matrix of \mathbf{b} becomes diagonal.

Assume the coefficients \mathbf{b} are estimated using an unbinned extended maximum likelihood (EML) [4], with likelihood function

$$l(\mathbf{b}) = \ln(L(\mathbf{b})) = \sum_{\mathbf{x}_i \sim p(\mathbf{x})} \ln(A^2(\mathbf{x}_i, \mathbf{b})) - n(\mathbf{b}). \quad (3)$$

By taking the second derivative of Equation (3) one can show that for the square root transform the coefficient covariance matrix converges towards a diagonal matrix with $1/4$ on the diagonal:

$$V^{-1}(\hat{\mathbf{b}})_{kl} = -\frac{\partial^2 \ln(L(\hat{\mathbf{b}}))}{\partial b_k \partial b_l} = \sum_{\mathbf{x}_i \sim p(\mathbf{x})} 2 \frac{\phi_k(\mathbf{x}_i) \phi_l(\mathbf{x}_i)}{A^2(\mathbf{x}_i, \hat{\mathbf{b}})} + 2\delta_{kl} \simeq 2 \int_V P(\mathbf{x}) \frac{\phi_k(\mathbf{x}) \phi_l(\mathbf{x})}{A^2(\mathbf{x}, \hat{\mathbf{b}})} d\mathbf{x} + 2\delta_{kl} \simeq 4\delta_{kl}$$

where $\hat{\mathbf{b}}$ is the EML estimate of the coefficients and the orthonormality of $\phi_k(\mathbf{x})$ as well as the assumption that $A^2(\mathbf{x}, \mathbf{b})$ point-wise approximates $P(\mathbf{x})$ have been used.

3.3 The square root SFI transform

The square root transform series $A(\mathbf{x}, \mathbf{b})$ can be found by applying event reweighting. This unfortunately requires knowledge of the function $A(\mathbf{x}, \mathbf{b})$ itself, which originally is unknown since that is the very function to be solved for in the first place. This recurrence problem can be circumvented assuming a start vector for the function and then finding the solution as the fix-point from successive iterations. The task in each iteration is to find $\mathbf{b}^{(n+1)}$ in $A(\mathbf{x}, \mathbf{b})$, given events of $P(\mathbf{x})$ and the previous suggestion $\mathbf{b}^{(n)}$. Inspired by

$$\int_V A(\mathbf{x}) \phi_u(\mathbf{x}) d\mathbf{x} = \int_V P(\mathbf{x}) \frac{\phi_u(\mathbf{x})}{A(\mathbf{x})} d\mathbf{x},$$

the reweighting during each iteration can be written

$$b_u^{(n+1)} = \sum_{\mathbf{x}_i \sim A(\mathbf{x})} \phi_u(\mathbf{x}_i) \simeq \sum_{\mathbf{x}_i \sim P(\mathbf{x})} \frac{\phi_u(\mathbf{x}_i)}{A(\mathbf{x}_i, \mathbf{b}^{(n)})}$$

where the initial guess is $b_0^{(0)} = \sqrt{N}$ and $b_{i \neq 0}^{(0)} = 0$. The convergence of the iterations are controlled by a convex combination with a relaxation parameter ω and an optional regularization parameter ϵ implemented as

$$b_u^{(n+1)} = (1 - \frac{\omega}{2}) b_u^{(n)} + \frac{\omega}{2} \sum_{\mathbf{x}_i \sim p(\mathbf{x})}^N \frac{\phi_u(\mathbf{x}_i)}{A(\mathbf{x}_i, \mathbf{b}^{(n)}) + \epsilon \text{sign}(A(\mathbf{x}_i, \mathbf{b}^{(n)}))}.$$

For $\omega = 1$ this coincides with the Newton method for solving the equation $P(\mathbf{b}) - A^2(\mathbf{b}) = 0$. In the examples below ω ranges between $0.25 - 1.0$.

3.4 Minimizing the interpolation uncertainty in higher dimensions

In higher dimensions, large amounts of training data is required to sufficiently outnumber the degrees of freedom present in the SFI series. For a monomial sparse series, the training dataset with N events in d dimensions must fulfil

$$Nd \gg \frac{(d+l)!}{l!d!}.$$

where l is the basis function maximum degree. This is in practice often difficult to achieve. There are several intuitive and well known techniques available to avoid too many degrees of freedom, a.k.a. overtraining and noise learning, which are effective also in the SFI context. The degrees of freedom can be regulated via the *meta parameters*, such as maximum degree. One powerful method to determine

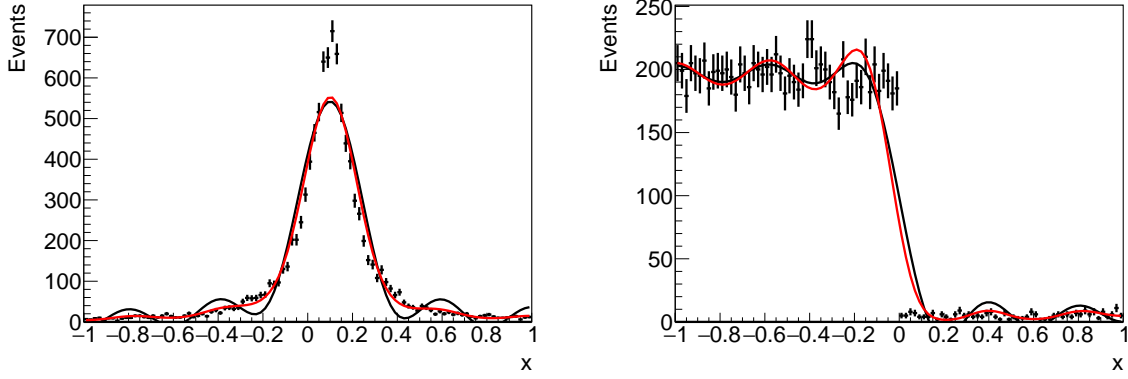


Figure 1: Histograms and SFI interpolations for Cauchy (left) and step (right) distributions with hard non-optimal Fourier coefficient truncation of the polynomial. The red curve is the square root SFI estimate. Note how the square root SFI transform remains non-negative by construction.

the values of the meta parameters is to minimize the *cross entropy* (H) as a function of the meta parameter in question. For samples drawn from the distribution $p(\mathbf{x})$ the cross entropy H with respect to the interpolated distribution $p(\mathbf{x}, \mathbf{b})$ can be estimated with:

$$H = -\frac{1}{N} \sum_{\mathbf{x}_i \sim p(\mathbf{x})} \ln(p(\mathbf{x}_i, \mathbf{b})).$$

For SFI the maximum degree of the polynomial (l) is a direct handle to control the degrees of freedom of the interpolation and regulate H . It is strongly advised to always work with SFI transformations that use the maximal degree determined from the optimum provided by the cross entropy minimum. The method still works with harder truncation of the maximum degree for the eigenfunctions, albeit with reduced performance. However a too high maximum degree results in the usual and familiar problems associated with overtraining. An additional way to improve the performance is to transform the input variables such that the required number of eigenfunctions are reduced.

3.5 Example distributions

Figure 1 show histograms of Cauchy (left) and step function (right) distributed scattered data compared to SFI interpolation under hard non-optimal Fourier coefficient truncation. The red curve is the square root SFI estimate. The series use cosine as basis functions and are truncated above degree 10. Both distributions are challenging in different ways, the Cauchy (Breit-Wigner) has a sharp peak while the step function is discontinuous. In both cases it can be seen that the linear SFI transform give a negative density estimate for some fraction of the interval.

Figure 2 show estimates of H as a function of the maximum degree for the two example distributions using 10k events. The red and green curves in the figure approximate H using a transform of even samples evaluated on odd samples, and vice verse. The black curve approximates H by 5-fold cross entropy where the average and uncertainty of the average is shown. In the n -fold cross entropy the transform is made out of each of n subsamples (defined by excluding the i :th event where i runs from 0 to 4) evaluated on the rest of the data. The optimal polynomial degree can be estimated from the minimal degree when H reaches its minimum. This gives $l \simeq 18$ for the Chauchy example and $l \simeq 34$ for the step example. The distributions in Figure 1 replaced with the estimated optimal truncation are shown in Figure 3.

4 Method validation: SFI for nonparametric density estimation

An optimal alternative to the SFI method described in the previous chapter, that is only tractable in low dimensions, is to directly estimate the Fourier coefficients \mathbf{b} using an unbinned EML, with likelihood

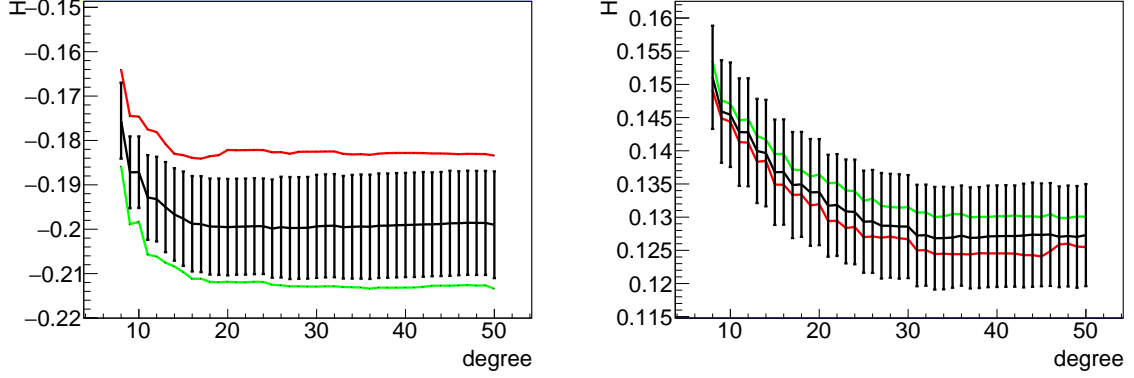


Figure 2: Estimates of the cross entropy for the Cauchy (left) and step (right) distributions. The red and green curves in the figure approximate H using a transform of even samples evaluated on odd samples, and vice verse. The black curve approximates H by 5-fold cross entropy where the average and uncertainty of the average is shown.

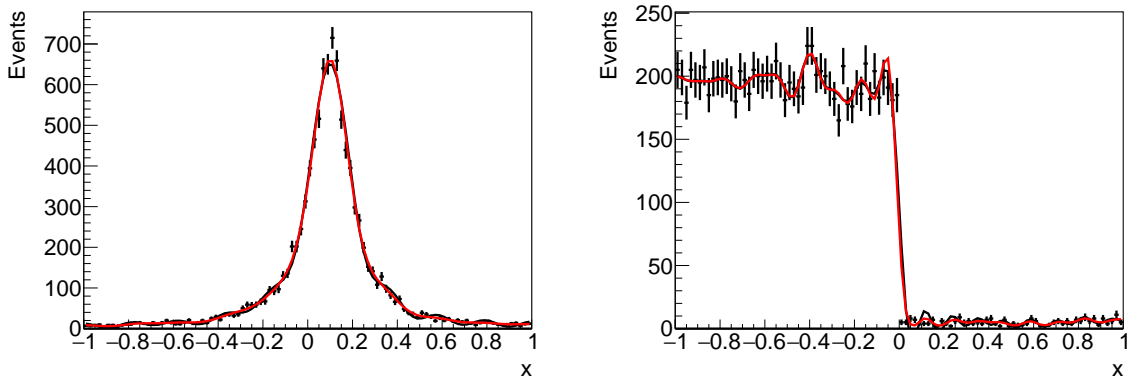


Figure 3: Histogram and optimal SFI interpolation for Cauchy (Breit-Wigner) and step distributions with maximum degree 18 and 34 respectively. The optimal degree is selected using the minimum degree of the series where the estimated cross entropy H reaches its minimum.

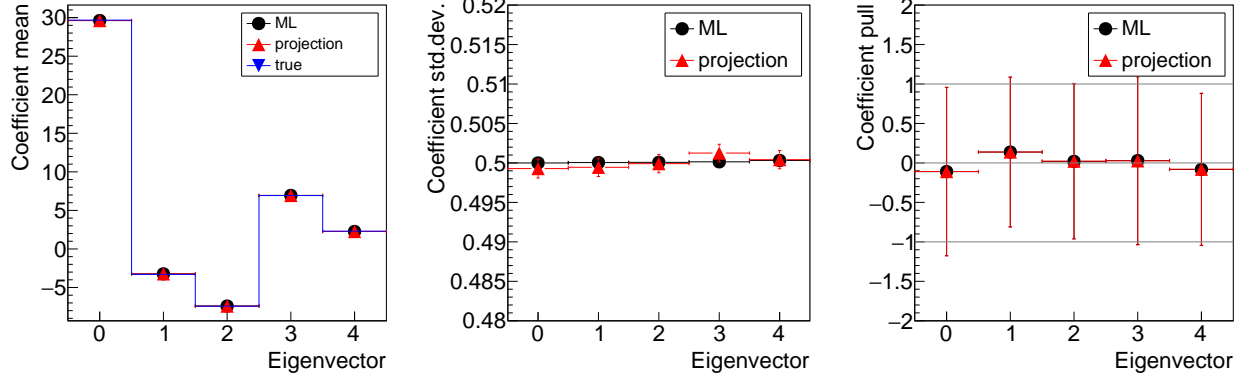


Figure 4: Comparing the performance of an extended maximal likelihood fit (EML) to the direct event projection method to calculate the SFI transform of five eigenvectors using Poisson(10k) distributed events and 200 pseudo experiments. The plots show the mean (left), standard deviation (middle), and pull (right).

function given by Equation (3). The algorithm MIGRAD from the package MINUIT [5] is used for the numerical minimizations. The density is estimated using a sample of Poisson(10k) distributed events generated from a density made out of five known orthonormal cosine eigenvectors. The performance of using either EML or SFI transformations are compared in Figure 4. The uncertainties for SFI are estimated using bootstrapping. The coefficients estimated with SFI are found to be statistically compatible with EML and consequently compatible with the Cramer-Rao bound.

That the covariance matrix becomes diagonal is confirmed by the estimated covariance matrix provided by the EML fit, and is in stark contrast to the linear transform where the Fourier coefficients are highly correlated and in general requires the full covariance matrix to be useful. However, as will be shown later, the covariance matrix for the linear transform can be computed from the coefficients.

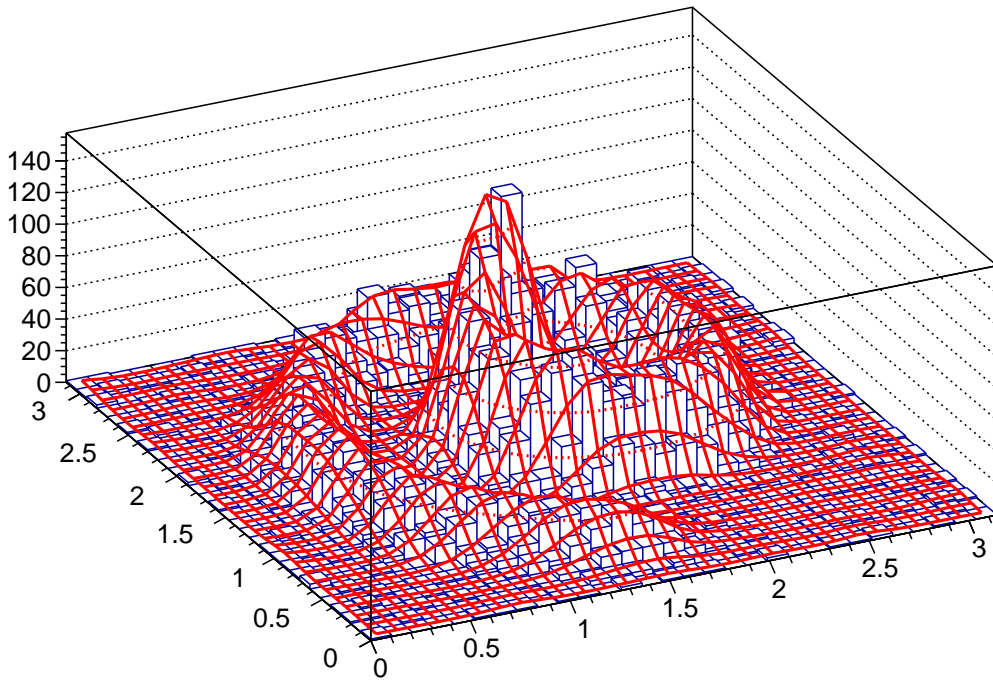


Figure 5: The spiral density estimated using SFI interpolation with $l = 15$ and 136 cosine eigenvectors.

The density of a more challenging 2D spiral distribution is shown in Figure 5. The density estimation is performed using a series with $l = 15$ giving 136 eigenfunctions, both using EML and SFI transform with compatible results. Given a computing time of less than a minute on a standard laptop the EML fit is practically limited to $O(100)$ eigenvectors, while the SFI transform limitation in the current implementation is $O(100k)$ eigenvectors. Using the numbers provided in Table 1 shows that this allows for access to domains that are normally out of reach, e.g. $d = 10$ and $l = 10$.

5 SFI example: classification

Given signal and background densities it is possible to perform classification. This is not the primary use-case for SFI but rather a way of comparing the performance of SFI to other well established techniques. The signal decision function is constructed from separate SFI transforms of the signal and background model events according to

$$s(\mathbf{x}) = \frac{n_s p_s(\mathbf{x})}{n_s p_s(\mathbf{x}) + n_b p_b(\mathbf{x})} = \frac{P_s(\mathbf{x})}{P_s(\mathbf{x}) + P_b(\mathbf{x})} \simeq \frac{P_s(\mathbf{x}, \mathbf{a}_s)}{P_s(\mathbf{x}, \mathbf{a}_s) + P_b(\mathbf{x}, \mathbf{a}_b)}.$$

In these examples $n_s = n_b$. The first example uses intertwined spirals of the type shown in the previous chapter, but in this case with $l = 12$ to limit overtraining. The classification boundary is highly nonlinear and cannot be well separated using only a naive Bayes classifier (LD) even if the input variables are de-correlated (LDD). The SFI transform is compared to neural networks (MLP), boosted decision trees (BDT) and LD(D) with respect to timing and classification performance. The alternative classifiers are evaluated with the TMVA framework [6]. Classification performance is measured as received operation characteristics (ROC) and area under ROC curve (AUC) in the test sub sample, see Table 2 and Figure 7. A comparison between the classification efficiencies for the different methods can be found in Appendix B. More details on the example are given in Appendix C.

The choice of $l = 12$ is a trade off between speed and accuracy. The cross entropy for this density as function of l is shown in Figure 6. As can be seen the choice of $l = 12$ is below the region where over training begins.

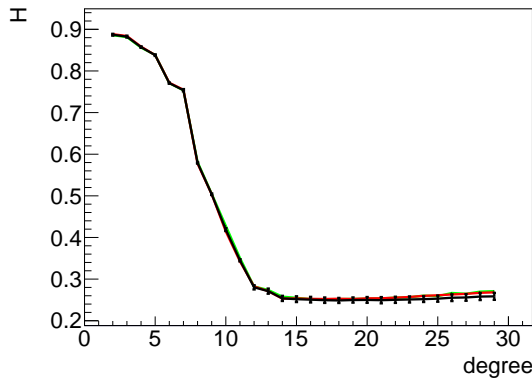


Figure 6: Estimates of the cross entropy for the the spiral density.

A second classification example is taken from high energy physics (HEP) to validate SFI in higher dimensions. The classification task is to separate top quark pairs from Z bosons in the dilepton plus at least one jet final state. The density has six dimensions: transverse momentum and η of the two leptons, invariant mass of the two leptons, and transverse momentum of the leading jet. The input variables are transformed for all methods, but for SFI the variables for $P_s(\mathbf{x}, \mathbf{a}_s)$ and $P_b(\mathbf{x}, \mathbf{a}_b)$ are transformed differently, since these densities are represented as different series and the extra variable transform can be applied with little additional cost. Classification performance is measured as ROC and AUC, see Table 3 and Figure 7. A comparison between the classification efficiencies for the different methods can be found in Appendix B. More details on the example are given in Appendix D.

	Training time (s)	Test time (s)	AUC Test
SFI	0.10	0.01	0.98
MLP	7.93	0.01	0.97
BDT	0.60	0.09	0.98
LD	0.00	0.00	0.65
LDD	0.01	0.01	0.65

Table 2: Spiral classification training time (for 10k events) and area under curve (AUC) numbers for different classifier methods.

	Training time (s)	Test time (s)	AUC Test
SFI	0.09	0.04	0.97
MLP	8.86	0.01	0.97
BDT	0.27	0.04	0.97
LD	0.01	0.00	0.88
LDD	0.02	0.01	0.88

Table 3: HEP classification training time and area under curve (AUC) numbers for different classifier methods.

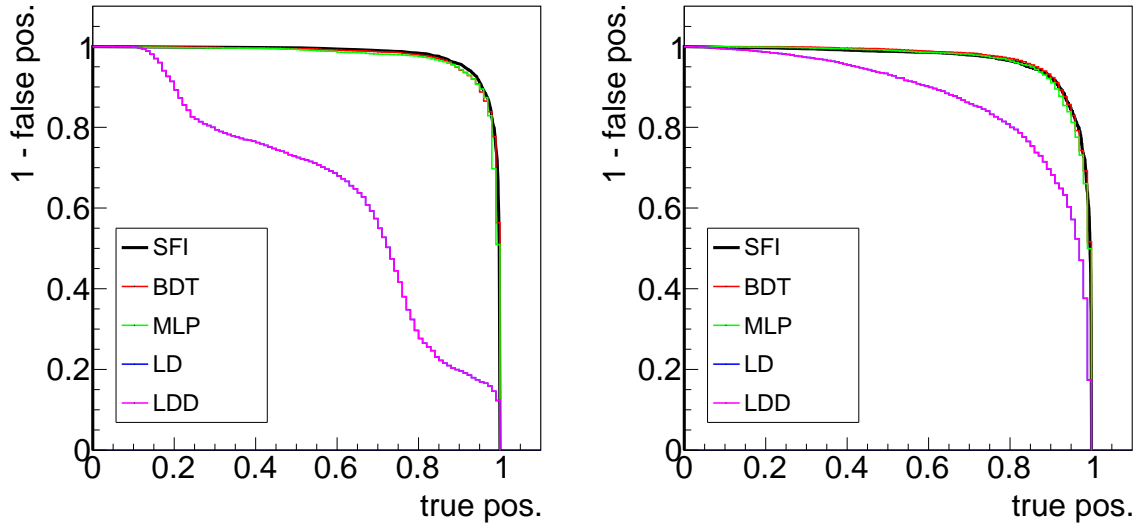


Figure 7: ROC curve for the spiral (left) and HEP (right) classification comparing SFI to other standard classifications methods: neural networks (MLP), boosted decision trees (BDT), naive Bayes classifier (LD) or de-correlated LD (LDD).

6 SFI example: parameter estimation

The examples below show two examples of parameter estimation. The parameter that is estimated is the mean of a Gaussian with a fixed standard deviation of $\sigma = 0.1$ on top of a exponentially falling background, with Poisson distributed numbers of data events. The fraction of the true signal and background events is a priori unknown and varied during the pull tests. The parameter estimation examples highlights two possible distinct working modes. In the first (default) case the model is SFI transformed into square root Fourier space and then inversely transformed back into the original x-space. This transformation and inverse transformation is how the interpolation of the original sampled model is achieved. The sampled data points are then compared to the interpolated density using an unbinned extended maximum likelihood.

In the second example both the model and the data are linearly SFI transformed into Fourier space and the analysis is performed entirely within Fourier space without any inverse transformation back to x-space.

6.1 Default SFI

The starting point is a transform describing the conditional pdf of the signal given the parameters \mathbf{c} : $p_s(\mathbf{x}_i|\mathbf{c})$. Depending on the model this transform is constructed in one of two ways. If model events are available uniformly covering the entire model parameter space for \mathbf{c} then $p_s(\mathbf{x}_i|\mathbf{c})$ can easily be constructed from the joint pdf $p_s(\mathbf{x}_i, \mathbf{c})$. If the model samples are given uniformly at certain discrete values of \mathbf{c} then the method outlined in section 6.1.1 can be used.

From the conditional pdf $p_s(\mathbf{x}_i|\mathbf{c}) = p_s(\mathbf{x}_i, \mathbf{b}(\mathbf{c}))$ it is straight forward to formulate the default SFI parameter estimation as an unbinned EML with likelihood

$$l(n_s, n_b, \mathbf{c}) = \ln(L(n_s, n_b, \mathbf{c})) = \sum_{i=1}^N \ln \left(\frac{n_s p_s(\mathbf{x}_i, \mathbf{b}(\mathbf{c})) + n_b p_b(\mathbf{x}_i)}{n_s + n_b} \right) + N \ln(n_s + n_b) - n_s - n_b,$$

where n_s and n_b are the model yields for the signal and background respectively, \mathbf{c} is the signal model parameter vector with corresponding Fourier coefficients $\mathbf{b}(\mathbf{c})$, and \mathbf{x}_i are the scattered data events. The signal and background Fourier coefficients are normalized such that the integrals of p_s and p_b are equal to one.

The standard deviation and pull from the parameter fit are shown in Figure 8 and compared to optimal performance. The parameter estimates are performed for 7 different values of \mathbf{c} . Figure 9 shows pull for \hat{n}_s and \hat{n}_b in pseudo experiments where the number of signal events (n_s) have been varied while keeping a fixed number of background events (n_b). The true parameter value \mathbf{c} is constant in this case.

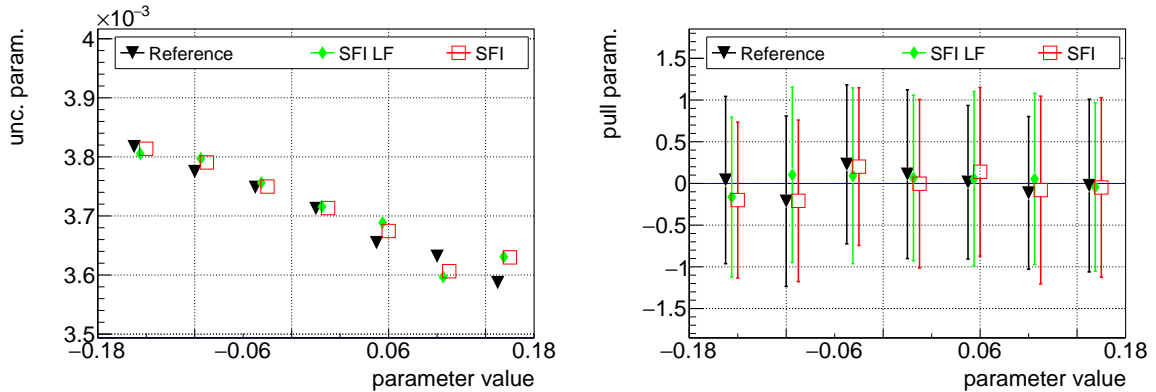


Figure 8: Uncertainty (left) and pull (right) for the parameter estimation example, comparing SFI to a reference provided by an unbinned fit of the original known function. 1k events are used for both signal and background.

6.1.1 When only discrete model point are available

When the model is only available at certain grid points, i.e. discrete values of \mathbf{c} , which is common when the model is given by Monte Carlo simulations, an interpolation can be performed as follows. First the Fourier coefficients are rewritten as a separate Fourier series $b_i(\mathbf{c}) = \sum_j c_{ij} \varphi_j(\mathbf{c})$. The eigenfunctions $\varphi_j(\mathbf{c})$ are tensor products of one dimensional Chebychev eigenfunctions. The cosine basis is used for \mathbf{x} , $\phi_j(\mathbf{x})$, and the full tensor product of $\varphi_j(\mathbf{c})$ and $\phi_j(\mathbf{x})$ is used to build the series for $p_s(\mathbf{x}_i, \mathbf{b}(\mathbf{c}))$. Before data can be fitted, the Fourier coefficients c_{ij} are first found by SFI transforming each model sample at \mathbf{c}_j and then solving a linear equation system, see Appendix A for details. This allows for interpolation between discrete model points in case the model parameters cannot be generated continuously. An interpolation example of the first coefficients in the series is shown in Figure 10. Note that this procedure can be applied to both the linear and square root transforms.

6.2 Linear SFI analysis in Fourier space

In many cases it can be very advantageous to perform the analysis only within Fourier space, i.e. use the Fourier coefficients instead of the function values at the original \mathbf{x}_i coordinates. Unfortunately the non-linear nature of the SFI square root transform does not allow the coefficients to be directly compared between different transformed distributions. Primarily due to different diagonalizations of the covariance matrix and rescalings taking place for each transform. However, in analogy with the characteristic function which provides an alternative representation of the probability distribution in

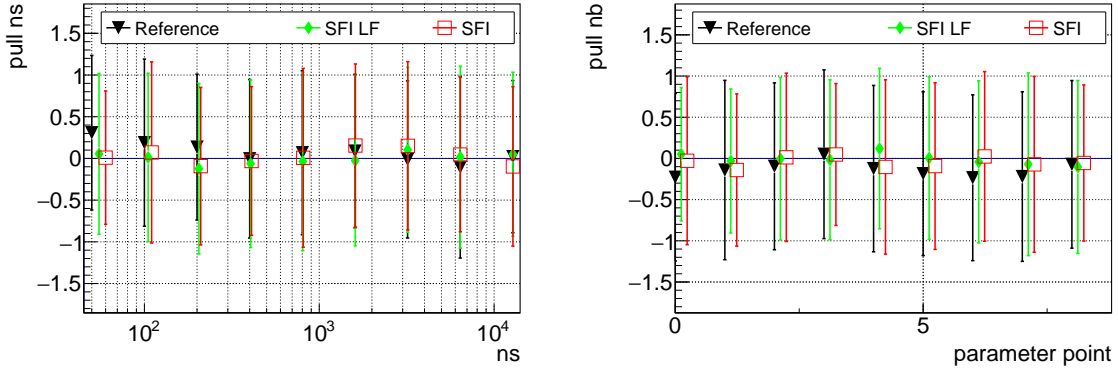


Figure 9: Pull for \hat{n}_s (left) and \hat{n}_b (right) in pseudo experiments where the values of n_s have been varied, while n_b was fixed. The value of the unknown parameter has been kept fixed.

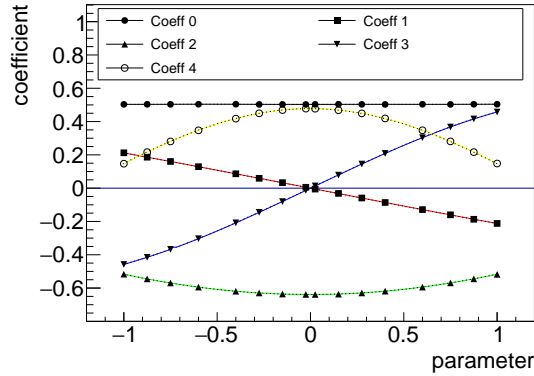


Figure 10: Coefficient interpolation for the square root transform as function of parameter value, in internal coordinates, between -1 and 1. Marked points are the coefficient values from the discrete model points while the line are the values interpolated from the combined transform derived with the technique outlined in Appendix A.

Fourier space, the linear version of SFI (see Equation (1)) allows for direct analysis in Fourier space.

The major drawback with linear SFI compared to default SFI is that the coefficients are no longer uncorrelated. The approach is based on the assumption that the linear SFI transformed coefficients are approximately distributed as a multivariate gaussian, which can be motivated by the central limit theorem. The linear SFI likelihood⁶ can then be written in Fourier space as

$$l(n_s, n_b, \mathbf{c}) = -2 \ln(L(n_s, n_b, \mathbf{c})) = -\ln |\Sigma^{-1}(n_s, n_b, \mathbf{c})| + \mathbf{r}(n_s, n_b, \mathbf{c})^T \Sigma^{-1}(n_s, n_b, \mathbf{c}) \mathbf{r}(n_s, n_b, \mathbf{c}), \quad (4)$$

where the residual $\mathbf{r}(n_s, n_b, \mathbf{c}) = \mathbf{d} - n_s \mathbf{b}_s(\mathbf{c}) - n_b \mathbf{b}_b$, and \mathbf{d} is the vector with filtered Fourier coefficients of the data. Both signal and background transforms are normalized to 1. This formulation requires the *precision matrix* $\Sigma^{-1}(n_s, n_b, \mathbf{c})$ to be specified, ideally analytically parameterized in the likelihood parameters n_s , n_b and \mathbf{c} . Since $\Sigma^{-1}(n_s, n_b, \mathbf{c})$ a priori is unknown it has to be estimated from the model, starting from an estimator $S(n_s, n_b, \mathbf{c})$ of the true covariance matrix $\Sigma(n_s, n_b, \mathbf{c})$. The estimated covariance matrix S consists of two terms, a Poisson distributed global normalization component Σ_n for a fixed normalized shape

$$\Sigma_n = n \mathbf{b}(\mathbf{c}) \mathbf{b}^T(\mathbf{c}),$$

and a noise component Σ_S for fixed n events with fluctuations only due to shape variations. According to Equation (1) the one event estimation of an eigenfunction is $\phi_k(\mathbf{x}_i) = b_k^i$. The noise components $(\Sigma_S)_{kl}$ can be measured using the sample covariance from each individual event as

$$\begin{aligned} (\Sigma_S)_{kl} &= n \cdot \text{cov}(b_k, b_l) = \frac{n}{N} \sum_{\mathbf{x}_i \sim p(\mathbf{x})} (b_k^i - b_k)(b_l^i - b_l) = \frac{n}{N} \sum_{\mathbf{x}_i \sim p(\mathbf{x})} b_k^i b_l^i - n b_k b_l \\ &= \frac{n}{N} \sum_{\mathbf{x}_i \sim p(\mathbf{x})} \phi_k(\mathbf{x}_i) \phi_l(\mathbf{x}_i) - n b_k b_l \end{aligned}$$

This implies that S can be written as

$$S_{kl} = (\Sigma_n)_{kl} + (\Sigma_S)_{kl} = \frac{n}{N} \sum_{\mathbf{x}_i \sim p(\mathbf{x})} \phi_k(\mathbf{x}_i) \phi_l(\mathbf{x}_i) \simeq n \langle \phi_k(\mathbf{x}) \phi_l(\mathbf{x}) \rangle_{p(\mathbf{x})}.$$

The computational complexity of S can further be drastically reduced by using the product rule of orthogonal eigenfunctions which are of the form

$$\phi_k \phi_l = \sum_{m(k,l)} g_m \phi_m,$$

for some set of constants g . This allows for S to be computed from the already modelled coefficients $\mathbf{b}(\mathbf{c})$ as

$$S_{kl} = \frac{n}{N} \sum_{\mathbf{x}_i \sim p(\mathbf{x})} \sum_{m(k,l)} g_m \phi_m(\mathbf{x}_i) = n \sum_{m(k,l)} g_m b_m(\mathbf{c}).$$

The covariance is composed of the covariances of the signal and background as:

$$S(n_s, n_b, \mathbf{c}) = (n_s + n_b) \left(\frac{n_s}{n_s + n_b} \tilde{S}_s(\mathbf{c}) + \frac{n_b}{n_s + n_b} \tilde{S}_b \right) = (n_s + n_b) \tilde{S}(n_s, n_b, \mathbf{c})$$

where $\tilde{S}_s(\mathbf{c})$ and \tilde{S}_b are computed from the normalized coefficients. The likelihood can now be written:

$$l(n_s, n_b, \mathbf{c}) = \dim(\tilde{\Sigma}^{-1}(n_s, n_b, \mathbf{c})) \ln(n_s + n_b) - \ln |\tilde{\Sigma}^{-1}(n_s, n_b, \mathbf{c})| + \frac{1}{n_s + n_b} \mathbf{r}(n_s, n_b, \mathbf{c})^T \tilde{\Sigma}^{-1}(\mathbf{c}) \mathbf{r}(n_s, n_b, \mathbf{c}).$$

The precision matrix $\Sigma^{-1}(\mathbf{c})$ is then robustly reconstructed using regularization provided by the ROPE [7] recipe, controlled by a tuning parameter α . The estimated covariance matrix S is eigendecomposed and the eigenvalues of Σ^{-1} are then computed (from the eigenvalues λ_i^S of S) as:

$$\lambda_i = \frac{2}{\lambda_i^S + \sqrt{(\lambda_i^S)^2 + 8\alpha}}$$

⁶Note that this likelihood contains a factor -2

unless $\lambda_i^S < 0.001 \times 8\alpha$, in which case $\lambda_i = 0$. The regularized Σ^{-1} corresponds to the maximum of the likelihood

$$l_{\text{reg}}(\Sigma^{-1}(n_s, n_b, \mathbf{c}), \alpha) = -\ln |\Sigma^{-1}(n_s, n_b, \mathbf{c})| + \text{Tr}(S\Sigma^{-1}(n_s, n_b, \mathbf{c})) + \alpha \|\Sigma^{-1}(n_s, n_b, \mathbf{c})\|_F^2$$

for all simulated events with a penalty term controlled by the regularization parameter α . The value of α is chosen to be 0.00001.

Finally the parameters are extracted by minimizing the likelihood

$$\arg \min_{n_s, n_b, \mathbf{c}} l(n_s, n_b, \mathbf{c}),$$

where the precision matrix is calculated in each step during the minimization. The results for this method (SFI LF) are shown in Figures 8 and 9.

7 Code implementation

A C++ library and examples for some of the SFI calculations explained in the text are available at the <https://gitlab.com/sfi-lib/libsfi> repository. This library contains several sets of eigenfunctions, e.g. the Fourier basis can be used for periodic variables, and spherical harmonics for a pair of variables possessing spherical symmetry. Functionality for choosing eigenfunction set, as well as order, for each dimension is available. Together with variable transformations (such as arctan or the logarithm) and methods for reducing overtraining this allows the transform to be tailored to the general features of a multidimensional distribution.

In addition, a transform can be integrated to obtain the marginal density for a single dimension. The marginal density can then be compared to an empirical distribution, either by eye or by using a statistical test.

8 Conclusions

A general and efficient method for analysis of events in higher dimensions using orthogonal real valued functions series is explained and exemplified. The range of applications is large and is not only limited to density estimation, classification or parameter estimation. In data analysis the reduction of degrees of freedom plays a central role. A powerful and important key property of SFI is that for both the square root and the linear transform the high degrees of freedom of the original scattered data is reduced and encapsulated solely by the SFI Fourier coefficients, no additional information is needed to specify the full covariance matrix among the coefficients.

The range of applications falls into two distinct classes: either the analysis is performed in the original x -space and only makes a visit in Fourier space and comes back again (see the classification example), or it leaves x -space completely and performs the analysis entirely in the linearly transformed Fourier space (see the second parameter estimation example). Note that the parameter correlations present in the linear transform case is a restriction due to increased complexity which is completely absent in the square root mode. However, low complexity can still be maintained in the linear case by carefully selecting the most relevant part of the spectrum from the signal point of view.

A C++ code library <https://gitlab.com/sfi-lib/libsfi> is provided with examples that allows for the reader to further explore other applications.

Acknowledgement

This work was funded in part by the Knut and Alice Wallenberg foundation under grant no. KAW 2017.0100.

References

- [1] Sam Efromovich. Orthogonal series density estimation. *WIREs Computational Statistics*, 2(4):467–476, 2010.
- [2] K.L. Judd et al. Approximation, perturbation, and projection methods in economic analysis. *Handbook of computational economics*, 1:509–585, 1996.
- [3] G.S. Watson et al. Density estimation by orthogonal series. *Ann. Math. Statist*, 40(4):1496–1498, 1969.
- [4] R.J. Barlow. Extended maximum likelihood. *Nucl. Instrum. Meth. A*, 297:496–506, 1990.
- [5] F. James. *MINUIT Function Minimization and Error Analysis: Reference Manual Version 94.1*, 1994. CERN-D-506.
- [6] A. Hocker et al. TMVA - Toolkit for Multivariate Data Analysis. 3 2007. CERN-OPEN-2007-007 physics/0703039.
- [7] M.O. Kuusmin, J.T. Kemppainen, and M.J. Sillanpää. Precision matrix estimation with rope. *Journal of Computational and Graphical Statistics*, 26(3):682–694, 2017.
- [8] J. Alwall, R. Frederix, S. Frixione, V. Hirschi, F. Maltoni, O. Mattelaer, H. S. Shao, T. Stelzer, P. Torrielli, and M. Zaro. The automated computation of tree-level and next-to-leading order differential cross sections, and their matching to parton shower simulations. *JHEP*, 07:079, 2014. 10.1007/JHEP07(2014)079.
- [9] Shi hai Dong and R. Lemus. The overlap integral of three associated legendre polynomials. *Applied Mathematics Letters*, 15(5):541–546, 2002.
- [10] *NIST Digital Library of Mathematical Functions*. <http://dlmf.nist.gov/>, Release 1.1.4 of 2022-01-15. F. W. J. Olver, A. B. Olde Daalhuis, D. W. Lozier, B. I. Schneider, R. F. Boisvert, C. W. Clark, B. R. Miller, B. V. Saunders, H. S. Cohl, and M. A. McClain, eds.
- [11] Giulio Racah, Eugen Merzbacher, and David Pank. *Group theory and spectroscopy*. Ergebnisse der exakten Naturwissenschaften. CERN, Geneva, 1961. Reprinted in: Ergebnisse der exakten Naturwissenschaften, Bd. 37 (1965), Springer.

Appendices

A Solving the model Fourier coefficients

The model, assumed to be dependent on the parameter vector \mathbf{c} , is given at a discrete number of model points \mathbf{c}_n and approximated as a finite Fourier series as

$$f(\mathbf{x}, \mathbf{c}_n) = \sum_{ij} f_{ij} \phi_i(x) \varphi_j(\mathbf{c}_n),$$

where $\varphi_j(\mathbf{c})$ here are chosen as Chebychev polynomials to maximize the approximation efficiency. The basis set can either be SFI or full tensor depending on the application. The model points can also be SFI transformed individually without \mathbf{c} dependence as

$$m^n(\mathbf{x}) = \sum_k m_k^n \phi_k(\mathbf{x}).$$

For a fixed model point \mathbf{c}_n both descriptions should agree such that (to reduce the notation $\varphi_j(\mathbf{c}_n) = \varphi_j^n$)

$$\sum_k m_k^n \phi_k(\mathbf{x}) = \sum_{ij} f_{ij} \phi_i(\mathbf{x}) \varphi_j^n.$$

This constraint can be turned into a equation system in Fourier space by projecting both sides on to the eigenfunction $\phi_l(\mathbf{x})$

$$\int \sum_k m_k^n \phi_k(\mathbf{x}) \phi_l(\mathbf{x}) d\mathbf{x} = \int \sum_{ij} f_{ij} \phi_i(\mathbf{x}) \varphi_j^n \phi_l(\mathbf{x}) d\mathbf{x},$$

which then becomes an equation system for the unknowns f_{ij}

$$m_l^n = \sum_j f_{lj} \varphi_j^n.$$

For $M = 3$ Fourier dimensions in \mathbf{x} and $N = 2$ Fourier dimensions in \mathbf{c} the components of the equation system are

$$\begin{aligned} m_0^0 &= \varphi_0^0 f_{00} + \varphi_1^0 f_{01} \\ m_1^0 &= \varphi_0^0 f_{10} + \varphi_1^0 f_{11} \\ m_2^0 &= \varphi_0^0 f_{20} + \varphi_1^0 f_{21} \\ m_0^1 &= \varphi_0^1 f_{00} + \varphi_1^1 f_{01} \\ m_1^1 &= \varphi_0^1 f_{10} + \varphi_1^1 f_{11} \\ m_2^1 &= \varphi_0^1 f_{20} + \varphi_1^1 f_{21}. \end{aligned}$$

In matrix form this reads

$$\begin{pmatrix} m_0^0 \\ m_1^0 \\ m_2^0 \\ m_0^1 \\ m_1^1 \\ m_2^1 \end{pmatrix} = \begin{pmatrix} \varphi_0^0 & \varphi_1^0 & 0 & 0 & 0 & 0 \\ \varphi_0^1 & \varphi_1^1 & 0 & 0 & 0 & 0 \\ 0 & 0 & \varphi_0^0 & \varphi_1^0 & 0 & 0 \\ 0 & 0 & \varphi_0^1 & \varphi_1^1 & 0 & 0 \\ 0 & 0 & 0 & 0 & \varphi_0^0 & \varphi_1^0 \\ 0 & 0 & 0 & 0 & \varphi_0^1 & \varphi_1^1 \end{pmatrix} \begin{pmatrix} f_{00} \\ f_{01} \\ f_{10} \\ f_{11} \\ f_{20} \\ f_{21} \end{pmatrix}.$$

From the structure of the components it is clear that the solution consists of M linear independent matrix equations, each of size $N \times N$. To solve the system at least N model points are needed. In practice one should use more than N points and use the least squares solution to project the data down on to the truncated Chebychev series.

B Classification comparisons

Tables 4 and 5 contain comparisons between signal efficiencies for the different classification methods. The signal efficiencies are computed at certain background efficiencies (0.01, 0.1 and 0.3), both for the test and training samples. The goal is not only to get a high signal efficiency, but also to get compatible efficiencies in the test and training samples, i.e. to reduce overtraining. The aim has been to make a fair comparison, in terms of speed and efficiency, but it might be possible to further optimize the MLP and BDT methods to achieve the same – or better – performance in less time. Classification is however, as stated before, not the primary goal of the SFI methods.

C Configuration for the 2D spiral example

The spirals are modelled by a 2-dimensional cosine transform with maximum degree 12, i.e. a monomic sparse tensor series. 10k events are used for both signal and background spiral, and half of the events are used for training and the other half for testing.

D Configuration for the HEP example

Both signal and background are modelled by a 6-dimensional transform of maximum degree 5. Over-training is limited by performing significance pruning at a level of 3, i.e. coefficients where the value divided by the uncertainty is less than 3.0 are set to 0. 10k events are used for both signal and background samples, and half of the events are used for training and the other half for testing. The samples have been generated with MadGraph[8]. The lepton transverse momentum p_T is smeared by a gauss with width:

$$\sqrt{(0.00038p_T)^2 + 0.015^2}.$$

Jet p_T is smeared by a gauss with width:

$$\sqrt{(0.5/\sqrt{E})^2 + 0.03^2}.$$

The variables are constructed from two leptons (with $\eta < 2.5$) and the leading jet ($\eta < 2.5$) in the events. In collider physics it is common to use four dimensional vectors for particle energy and momentum, with components: E , p_T , η and φ , where the momentum part is given as cylindrical coordinates with the z-axis along the axis of the colliding beams. The transverse momentum (p_T) is the component of the momentum perpendicular (or transverse) to the z-axis. The pseudorapidity (η) is, for approximately mass less particles, defined as $\eta = -\ln \tan \theta/2$, where θ is the angle between the particle momentum and the z-axis. φ is the direction of the particle momentum in the x-y-plane.

The first variables are the lepton p_T that are required to be in the range 20 to 100 GeV and they are log transformed. The third variable is the leading jet p_T which is required to be in the range 20 to 200 GeV and is log transformed. The fourth variable is the invariant mass of the leptons, required to be in the range 21 to 161 GeV, and it is arctan transformed. The fifth and sixth variables are the lepton η that are arctan transformed. For SFI the variable transformation types are the same but the parameters are different for the signal and background samples.

E Fourier and spherical harmonics bases

Two sets of complex basis functions will be treated: The Fourier basis

$$F_l(\phi) = n_l e^{il\pi\phi} \quad (5)$$

and spherical harmonics

$$Y_l^m(x, \phi) = n_l^m P_l^m(x) e^{im\pi\phi}. \quad (6)$$

	Test @0.01	Train @0.01	Test @0.10	Train @0.10	Test @0.30	Train @0.30
SFI	0.71	0.72	0.96	0.96	0.99	0.99
MLP	0.55	0.63	0.95	0.95	0.99	0.99
BDT	0.62	0.67	0.95	0.95	0.99	0.99
LD	0.13	0.14	0.20	0.20	0.57	0.54
LDD	0.13	0.14	0.20	0.20	0.57	0.54

Table 4: Spiral signal efficiency for different background efficiencies

	Test @0.01	Train @0.01	Test @0.10	Train @0.10	Test @0.30	Train @0.30
SFI	0.44	0.45	0.92	0.93	0.99	0.99
MLP	0.52	0.54	0.91	0.91	0.98	0.98
BDT	0.57	0.66	0.92	0.93	0.98	0.99
LD	0.17	0.16	0.60	0.61	0.89	0.91
LDD	0.17	0.16	0.60	0.61	0.89	0.91

Table 5: HEP signal efficiency for different background efficiencies

With variables $-1 \leq \phi \leq 1$ and $-1 \leq x \leq 1$. n_l and n_l^m are normalizations factors and they will be discussed below. P_l^m are associated Legendre polynomials (ALP:s) that include the Condon-Shortley phase $(-1)^m$. Both basis functions have the property that ϕ is periodic.

In most cases the variables will be omitted from the basis functions, F_l, Y_l^m, φ_l , unless special attention is needed. φ_l will be used to denote a generic orthonormal basis function. Complex conjugation will be denoted \bar{c} . Unless specified, the indices in the series are summed as full tensors from 0 to N , where N is the maximum order of the basis functions, or as monomic sparse series.

Internally, in the SFI library, variables are transformed to the interval $(-1, 1)$, either by a linear transformation or by one of the non-linear transformations. For the complex exponential the integral becomes:

$$\int_{-1}^1 e^{im\pi\phi} d\phi = 2\delta_{m0}. \quad (7)$$

E.1 Marginalizations

In some situations it is desirable to perform marginalizations of a pdf of several variables. Besides statistical applications, e.g. a Kolmogorov-Smirnov test to data, it allows for visualization of the distributions and comparison to data by eye.

For a linear transform, the marginal pdf is expressed using the integral (I) of the eigenfunctions:

$$\begin{aligned} p(x_1, \mathbf{b}) &= \sum_l b_l \varphi_l(x_1) = \int p(\mathbf{x}, \mathbf{a}) dx_2 \dots dx_d \\ &= \int \sum_{l_1 \dots l_d} a_{l_1 \dots l_d} \varphi_{l_1}(x_1) \dots \varphi_{l_d}(x_d) dx_2 \dots dx_d = \sum_{l_1 \dots l_d} a_{l_1 \dots l_d} \varphi_{l_1}(x_1) I_{l_2} \dots I_{l_d} \end{aligned}$$

For the square root transform, since the eigenfunctions are required to be orthonormal, the marginalization procedure is simplified:

$$\begin{aligned} p(x_1, \mathbf{b}) &= \int p(\mathbf{x}, \mathbf{a}) dx_2 \dots dx_d = \int A(\mathbf{x}, \mathbf{a})^2 dx_2 \dots dx_d \\ &= \sum_{l_1 \dots l_d} \sum_{k_1 \dots k_d} a_{l_1 \dots l_d} a_{k_1 \dots k_d} \int \varphi_{l_1}(x_1) \dots \varphi_{l_d}(x_d) \varphi_{k_1}(x_1) \dots \varphi_{k_d}(x_d) dx_2 \dots dx_d \\ &= \sum_{l_1 \dots l_d} \sum_{k_1} a_{l_1 \dots l_d} a_{k_1 l_2 \dots l_d} \varphi_{l_1}(x_1) \varphi_{k_1}(x_1) \end{aligned}$$

The next step is to turn the product $\varphi_l \varphi_k$ into a sum of single φ_l . Such relations exist for Legendre polynomials and cosine, as well as for Fourier and spherical harmonics.

The marginalization procedure will thus turn a sqrt transform of several variables into a linear transform of fewer variables. Currently 1D and 2D marginalizations are supported, i.e. all but one or two variables may be integrated out.

E.2 Fourier

The implementation uses complex Fourier eigenfunctions. This means that both coefficients and eigenfunctions are complex in the transform:

$$p(x) \simeq \sum_{l=-N}^N a_l F_l.$$

Note that the index runs from negative to positive. However, since the transformed functions for both the linear and the square root transform are strictly real, there exists a reality constraint on the coefficients: $a_{-l} = \bar{a}_l$. Hence the the expansion for a linear transform can be written as:

$$p(x, \mathbf{a}) = a_0 F_0 \dots + a_l F_l + \bar{a}_l \bar{F}_l + \dots = a_0 F_0 + \sum_l 2\text{re}\{a_l F_l\}.$$

This implies that the coefficients for negative l are not needed (but it does *not* imply that the coefficients are real.) A can also be written in terms of only positive l :

$$A(x, \mathbf{b}) = b_0 \varphi_0 + 2 \operatorname{re} \left\{ \sum_{l=1}^N b_l F_l \right\}.$$

To simplify the expressions, the eigenfunctions are scaled according to:

$$\tilde{\varphi}_l(x) = c_l \varphi_l(x) \quad c_l = \sqrt{2 - \delta_{l0}}.$$

A new set of coefficients for both the linear and the sqrt transform is obtained:

$$\tilde{b}_l = c_l b_l.$$

Expressed in the scaled coefficients and eigenfunctions the sqrt transform becomes:

$$A(x, \mathbf{b}) = \operatorname{re} \left\{ \sum_l 2d_l b_l F_l \right\} = \operatorname{re} \left\{ \sum_l \tilde{b}_l \tilde{F}_l \right\}. \quad (8)$$

where d_l has been introduced:

$$d_l = \frac{1}{1 + \delta_{l0}}.$$

with the property $2d_l = c_l^2$.

The normalization factor n_l is given by the integral (7) to be $1/\sqrt{2}$, and the scaled normalization becomes

$$\tilde{n}_l = c_l n_l = \frac{1}{\sqrt{1 + \delta_{l0}}}.$$

E.2.1 Marginalization

To properly account for coefficients with negative indices, rewrite (8) in terms of the unscaled coefficients and eigenfunctions and take the square:

$$A(x, \mathbf{b})^2 = \sum_{lk} d_l d_k (b_l F_l + b_{-l} F_{-l})(b_k F_k + b_{-k} F_{-k}).$$

Introduce $g_{lk} = b_l b_k F_l F_k = g_{kl}$ with properties $\bar{g}_{lk} = g_{-l-k}$ and $\bar{\bar{g}}_{-lk} = g_{l-k}$:

$$A(x, \mathbf{b})^2 = \sum_{lk} d_l d_k (g_{lk} + g_{l-k} + g_{-lk} + g_{-l-k}) = \sum_{lk} 2d_l d_k \operatorname{re}\{g_{lk} + g_{l-k}\}.$$

By using that $g_{lk} = g_{kl}$ and introducing a symmetry factor $e_{lk} = 2 - \delta_{lk}$, the series can be rewritten:

$$A(x, \mathbf{b})^2 = \operatorname{re} \left\{ \sum_{lk}^{k \leq l} 2d_l d_k e_{lk} (g_{lk} + g_{l-k}) \right\}.$$

The gain of this expression is that by exploiting symmetries, fewer operations have to be performed.

It now remains to reintroduce scaled coefficients and eigenfunctions. Products of Fourier eigenfunctions can be expressed as single eigenfunctions:

$$F_l F_k = n_l n_k e^{i(l+k)\pi\phi} = \frac{n_l n_k}{n_{l+k}} F_{l+k}.$$

Which gives that:

$$A(x, \mathbf{b})^2 = \operatorname{re} \left\{ \sum_{lk}^{k \leq l} 2d_l d_k e_{lk} \left(b_l b_k \frac{n_l n_k}{n_{l+k}} F_{l+k} + b_l b_{-k} \frac{n_l n_k}{n_{l-k}} F_{l-k} \right) \right\}.$$

With scaled coefficients and eigenfunctions:

$$\begin{aligned} A(x, \mathbf{b})^2 &= \text{re} \left\{ \sum_{lk}^{k \leq l} \frac{2d_l d_k e_{lk} \tilde{n}_l \tilde{n}_k}{c_l^2 c_k^2} \left(\frac{\tilde{b}_l \tilde{b}_k}{\tilde{n}_{l+k}} \tilde{F}_{l+k} + \frac{\tilde{b}_l \tilde{b}_k}{\tilde{n}_{l-k}} \tilde{F}_{l-k} \right) \right\} \\ &= \text{re} \left\{ \sum_{lk}^{k \leq l} \frac{e_{lk} \tilde{n}_l \tilde{n}_k}{2} \left(\frac{\tilde{b}_l \tilde{b}_k}{\tilde{n}_{l+k}} \tilde{F}_{l+k} + \frac{\tilde{b}_l \tilde{b}_k}{\tilde{n}_{l-k}} \tilde{F}_{l-k} \right) \right\}. \end{aligned}$$

The advantage of this last expression is that the coefficients for the linear transform all have positive indices and are given in terms of the scaled coefficients.

E.3 Spherical harmonics

The usual definition of $Y_l^m(x, \phi)$ is in terms of the angle θ such that $x = \cos(\theta)$, but the derivations will be clearer if this association is left out. The proper transformation will be achieved by making a variable transformation using cosine.

Spherical harmonics (6) are defined for negative m , and those functions are related to the conjugate functions:

$$\bar{Y}_l^m = (-1)^m Y_l^{-m}. \quad (9)$$

The linear transform can be written:

$$p(x, \phi, \mathbf{a}) = \sum_{lm}^{-l \leq m \leq l} a_{lm} Y_l^m.$$

We have that:

$$a_{l-m} = (-1)^m \bar{a}_{lm}$$

and the coefficients for negative m can be omitted, since:

$$\begin{aligned} p(x, \phi, \mathbf{a}) &= \sum_{lm}^{0 \leq m \leq l} d_m (a_{lm} Y_l^m + a_{l-m} Y_l^{-m}) \\ &= \sum_{lm}^{0 \leq m \leq l} d_m (a_{lm} Y_l^m + \bar{a}_{lm} \bar{Y}_l^m) \\ &= \text{re} \left\{ \sum_{lm}^{0 \leq m \leq l} 2d_m a_{lm} Y_l^m \right\} = \text{re} \left\{ \sum_{lm}^{0 \leq m \leq l} \tilde{a}_{lm} \tilde{Y}_l^m \right\} \end{aligned} \quad (10)$$

Scaled coefficients and basis functions were introduced in the last step.

The normalization of Y_l^m is given by:

$$\begin{aligned} \int Y_l^m \bar{Y}_l^m d\Omega &= \int_{-1}^1 Y_l^m \bar{Y}_l^m dx d\phi = \int_{-1}^1 (n_l^m)^2 P_l^m P_l^m dx d\phi = \frac{2(n_l^m)^2 2(l+m)!}{(2l+1)(l-m)!} = 1. \\ n_l^m &= \sqrt{\frac{(2l+1)(l-m)!}{4(l+m)!}} \end{aligned}$$

This differs from the usual normalization by a factor of $1/\sqrt{\pi}$ due to the different domain for ϕ . With scaling, the normalization becomes:

$$\tilde{n}_l^m = c_m n_l^m.$$

E.3.1 Marginalization of a linear transform

Expanding (10) in terms of the components of Y_l^m (6) gives:

$$p(x, \phi, \mathbf{a}) = \text{re} \left\{ \sum_{lm}^{0 \leq m \leq l} c_m^2 a_{lm} n_l^m P_l^m e^{im\pi\phi} \right\}.$$

The marginalization in x is given by:

$$p(x, \mathbf{b}) = \int_{-1}^1 p(x, \phi, \mathbf{a}) d\phi = \text{re} \left\{ \sum_{lm}^{0 \leq m \leq l} c_m^2 a_{lm} n_l^m P_l^m 2\delta_{m0} \right\} = \text{re} \left\{ \sum_l 2a_{l0} n_l^0 P_l^0 \right\}.$$

This is a series in Legendre polynomials(P_l), where the coefficients and eigenfunctions are real:

$$p(x, \mathbf{b}) = \sum_l b_l P_l = \sum_l \frac{2a_{l0} n_l^0}{n_l^P} P_l \quad b_l = \frac{2a_{l0} n_l^0}{n_l^P}$$

where n_l^P are the normalization factors for Legendre polynomials.

The marginalization in ϕ involves integrals of ALP:s:

$$p(\phi, \mathbf{b}) = \int_{-1}^1 p(x, \phi, \mathbf{a}) dx = \text{re} \left\{ \sum_{lm}^{0 \leq m \leq l} c_m^2 a_{lm} n_l^m e^{im\pi\phi} \int_{-1}^1 P_l^m dx \right\}.$$

The ALP integral is computed as [9]:

$$\int_{-1}^1 P_l^m dx = \frac{((-1)^m + (-1)^l) 2^{m-2} m \Gamma(l/2) \Gamma((l+m+1)/2)}{((l-m)/2)! \Gamma((l+3)/2)} = I_l^m. \quad (11)$$

Reverting to scaled coefficients:

$$p(\phi, \mathbf{b}) = \text{re} \left\{ \sum_{lm}^{0 \leq m \leq l} \frac{\tilde{a}_{lm} \tilde{n}_l^m I_l^m}{\tilde{n}_m} \tilde{F}_m \right\}.$$

This shows that the marginalization results in a linear Fourier series.

E.3.2 Marginalization of a sqrt transform

The sqrt transform in spherical harmonics is written as:

$$A(x, \phi, \mathbf{a})^2 = \sum_{lmkn} d_m d_n (a_{lm} Y_l^m + \bar{a}_{lm} \bar{Y}_l^m) (a_{kn} Y_k^n + \bar{a}_{kn} \bar{Y}_k^n).$$

Introducing $g_{lmkn} = a_{lm} a_{kn} Y_l^m Y_k^n$ gives:

$$A(x, \phi, \mathbf{a})^2 = \sum_{lmkn} d_m d_n (g_{lmkn} + g_{l-mkn} + g_{lmk-n} + g_{l-mk-n}).$$

Using the properties of the coefficients and basis functions we have $g_{l-mkn} = \bar{g}_{lmk-n}$ and $g_{l-mk-n} = \bar{g}_{lmkn}$.

$$A(x, \phi, \mathbf{a})^2 = \sum_{lmkn} d_m d_n (g_{lmkn} + \bar{g}_{lmkn} + g_{lmk-n} + \bar{g}_{lmk-n}) = \text{re} \left\{ \sum_{lmkn} 2d_m d_n (g_{lmkn} + g_{lmk-n}) \right\}.$$

If the serie is required to only have positive m , then one has to impose the condition $n \leq m$ and introduce the symmetry factor $e_{mn} = 2 - \delta_{mn}$. Expanding g_{lmkn} and using that $a_{k-n} = (-1)^n \bar{a}_{kn}$ gives:

$$A(x, \phi, \mathbf{a})^2 = \text{re} \left\{ \sum_{lmkn}^{n \leq m} 2e_{mn} d_m d_n (a_{lm} a_{kn} Y_l^m Y_k^n + (-1)^n a_{lm} \bar{a}_{kn} Y_l^m Y_k^{-n}) \right\}. \quad (12)$$

The relation (12) has three applications: Marginalization of a multidimensional transform into a linear 2D transform in x and ϕ and into a 1D transform of either x or ϕ .

For the first case, the product of two spherical harmonics can be turned into a sum of single spherical harmonics. Begin with the expression for a product of two ALP:s [9]:

$$P_l^m P_k^n = \sqrt{\frac{(l+m)!(k+n)!}{(l-m)!(k-n)!}} \sum_{L=\max(M, |l-k|)}^{l+k} \sqrt{\frac{(L-M)!}{(L+M)!}} C_{000}^{lkL} C_{mnM}^{lkL} P_L^M. \quad (13)$$

Where $M = m + n$, C_{mnM}^{lkL} are Clebsch-Gordan coefficients, and the constraint $M \leq L$ has been explicitly included. With this the expression for the product of the spherical harmonics can be written

$$Y_l^m Y_k^n = \sqrt{\frac{(2l+1)(2k+1)}{16}} \sum_{L=\max(M, |l-k|)}^{l+k} \sqrt{\frac{4}{(2L+1)}} C_{000}^{lkL} C_{mnM}^{lkL} Y_L^M \quad (14)$$

$$= \sum_{L=\max(M, |l-k|)}^{l+k} q_{lmknL} Y_L^M. \quad (15)$$

Note the difference in normalization.

Using this in the expression for A gives:

$$\begin{aligned} & A(x, \phi, \mathbf{a})^2 \\ &= \text{re} \left\{ \sum_{lmkn}^{n \leq m} 2e_{mn} d_m d_n \left(a_{lm} a_{kn} \sum_L q_{lmknL} Y_L^{m+n} + (-1)^n a_{lm} \bar{a}_{kn} \sum_L q_{lmk-nL} Y_L^{m-n} \right) \right\} \\ &= \text{re} \left\{ \sum_{lmkn}^{n \leq m} \frac{2e_{mn} d_m d_n}{c_m c_n} \left(\tilde{a}_{lm} \tilde{a}_{kn} \sum_L \frac{q_{lmknL}}{c_{m+n}} \tilde{Y}_L^{m+n} + (-1)^n \tilde{a}_{lm} \bar{\tilde{a}}_{kn} \sum_L \frac{q_{lmk-nL}}{c_{m-n}} \tilde{Y}_L^{m-n} \right) \right\} \end{aligned}$$

where L is summed from $\max(M, |l-k|)$ to $l+k$. This expression can be used to implement marginalization of a multi dimensional transform containing spherical harmonics.

Turning to the marginalization in x , expanding (12) in the parts of Y_l^m gives:

$$\begin{aligned} & \int A(x, \phi, \mathbf{a})^2 d\phi = \\ & \text{re} \left\{ \sum_{lmkn}^{n \leq m} 2e_{mn} d_m d_n n_l^m n_k^n \left(a_{lm} a_{kn} P_l^m P_k^n \int_{-1}^1 e^{i(m+n)\pi\phi} d\phi + a_{lm} \bar{a}_{kn} P_l^m P_k^n \int_{-1}^1 e^{i(m-n)\pi\phi} d\phi \right) \right\} \end{aligned}$$

The integral of the complex exponentials are only nonzero for the first term if $m+n=0$ and $m-n=0$ for the second. Since both m and n are positive we have $2\delta_{mn}\delta_{m0}$ for the first term and $2\delta_{mn}$ for the second. Both have the condition that $m \leq k$ in addition to $m \leq l$. It then follows that:

$$\begin{aligned} & \int A(x, \phi, \mathbf{a})^2 d\phi = \text{re} \left\{ \sum_{lmk}^{m \leq k} 4e_{mm} d_m d_m n_l^m n_k^m (a_{lm} a_{km} P_l^m P_k^m \delta_{m0} + a_{lm} \bar{a}_{km} P_l^m P_k^m) \right\} \quad (16) \\ &= \text{re} \left\{ \sum_{lmk}^{m \leq k} \frac{4d_m d_m \tilde{n}_l^m \tilde{n}_k^m}{c_m^4} (\tilde{a}_{lm} \tilde{a}_{km} P_l^m P_k^m \delta_{m0} + \tilde{a}_{lm} \bar{\tilde{a}}_{km} P_l^m P_k^m) \right\} \\ &= \text{re} \left\{ \sum_{lmk}^{m \leq k} \tilde{n}_l^m \tilde{n}_k^m (\tilde{a}_{lm} \tilde{a}_{km} P_l^m P_k^m \delta_{m0} + \tilde{a}_{lm} \bar{\tilde{a}}_{km} P_l^m P_k^m) \right\} \end{aligned}$$

Using (13), the last expression can be turned into a linear transform of ALP:s. The use of this transform is limited however, since the ALP:s are *not* orthonormal.

The marginalization in ϕ is given by a transform in the Fourier basis:

$$\int A(x, \phi, \mathbf{a})^2 dx = \text{re} \left\{ \sum_{lmkn}^{n \leq m} 2e_{mn} d_m d_n n_l^m n_k^n \left(a_{lm} a_{kn} e^{i(m+n)\pi\phi} \int P_l^m P_k^n dx + a_{lm} \bar{a}_{kn} e^{i(m-n)\pi\phi} \int P_l^m P_k^n dx \right) \right\}$$

Using (13) and (11) the integral of two ALP:s (I_{lk}^{mn}) can be computed, which gives:

$$\begin{aligned} \int A(x, \phi, \mathbf{a})^2 dx &= \text{re} \left\{ \sum_{lmkn}^{n \leq m} \frac{2e_{mn} d_m d_n \tilde{n}_l^m \tilde{n}_k^n I_{lk}^{mn}}{c_m^2 c_n^2} \left(\frac{\tilde{a}_{lm} \tilde{a}_{kn}}{\tilde{n}_{m+n}} \tilde{F}_{m+n} + \frac{\tilde{a}_{lm} \tilde{a}_{kn}}{\tilde{n}_{m-n}} \tilde{F}_{m-n} \right) \right\} \\ &= \text{re} \left\{ \sum_{lmkn}^{n \leq m} \frac{e_{mn} \tilde{n}_l^m \tilde{n}_k^n I_{lk}^{mn}}{2} \left(\frac{\tilde{a}_{lm} \tilde{a}_{kn}}{\tilde{n}_{m+n}} \tilde{F}_{m+n} + \frac{\tilde{a}_{lm} \tilde{a}_{kn}}{\tilde{n}_{m-n}} \tilde{F}_{m-n} \right) \right\} \end{aligned}$$

E.4 Computations

In (6) there are three quantities that need to be computed. The fourier factor is computed using:

$$F_n = 2 \cos(\pi\phi) F_{n-1} - F_{n-2}$$

with $F_0 = 1$ and $F_1 = e^{i\pi\phi}$.

The ALP is computed using the following, which can be found in [10] or derived from relations found there:

$$\begin{aligned} P_l^{l-1} &= x(2l-1)P_{l-1}^{l-1} \\ P_l^l &= -\sqrt{1-x^2}(2l-1)P_{l-1}^{l-1} \\ P_l^m &= \frac{-1}{(l+m+1)(l-m)} \left(2 \frac{(m+1)x}{\sqrt{1-x^2}} P_l^{m+1} + P_l^{m+2} \right) \end{aligned}$$

with the initial values:

$$P_0^0 = 1 \quad P_1^0 = x \quad P_1^1 = -\sqrt{1-x^2}.$$

There are alternative recursion relations, but the one chosen was found to be more accurate than a recursion starting with $m = 0$.

The Clebsh-Gordan coefficients are computed in a dense table. There are symmetry properties:

$$C_{mnM}^{klL} = (-1)^{l+k-L} C_{nmM}^{klL} = (-1)^{l+k-L} C_{(-n)(-m)(-M)}^{klL}$$

from which we can determine $k \leq l$ and $0 \leq M$, i.e. we do not need to compute coefficients with $M < 0$ or $k > l$. Further there are constraints:

$$-l \leq m \leq l \quad -k \leq n \leq k$$

$$l-k \leq L \leq l+k \quad 0 \leq M = m+n \leq L$$

From the last constraint it is clear that n (or m) can be omitted. Note that m and n are allowed to take on negative values. Using $n = M - m$ there are two constraints on m : $-k \leq M - m \leq k$ and $-l \leq m \leq l$. The first one can be written as $M - k \leq m \leq M + k$. Examining the lower bound reveals that $-l \leq M - k$ since $k \leq l$ and $0 \leq M$. The number of coefficients can be found from:

$$N_c = \sum_{l=0}^N \sum_{k=0}^{k \leq l} \sum_{L=l-k}^{l+k} \sum_{M=0}^L \sum_{m=M-k}^{\min(l, M+k)} 1$$

where N is the maximum number for l . An index in the table may be computed from this:

$$\begin{aligned}
I(l, k, L, M, m) = & \sum_{l'=0}^{l-1} \sum_{k'=0}^{k' \leq l'} \sum_{L'=l'-k'}^{l'+k'} \sum_{M'=0}^{L'} \sum_{m'=M'-k'}^{\min(l', M'+k')} 1 + \sum_{k'=0}^{k-1} \sum_{L'=l'-k'}^{l'+k'} \sum_{M'=0}^{L'} \sum_{m'=M'-k'}^{\min(l', M'+k')} 1 \\
& + \sum_{L'=l'-k'}^{L-1} \sum_{M'=0}^{L'} \sum_{m'=M'-k'}^{\min(l', M'+k')} 1 + \sum_{M'=0}^{M-1} \sum_{m'=M'-k'}^{\min(l', M'+k')} 1 + \sum_{m'=M'-k'}^{m-1} 1
\end{aligned}$$

The actual computations of the coefficients are done using recursion relations from [11]:

$$C_{\pm}(L, M)C_{mn(M \pm 1)}^{lkL} = C_{\pm}(l, m \mp 1)C_{(m \mp 1)nM}^{lkL} + C_{\pm}(k, n \mp 1)C_{m(n \mp 1)M}^{lkL} \quad (17)$$

with:

$$C_{\pm}(l, m) = \sqrt{l(l+1) - m(m \pm 1)}.$$

The initial recursion relation can be found by using (17) with $M = L$ and C_+ :

$$\begin{aligned}
0 = C_+(l, m-1)C_{(m-1)(n+1)L}^{lkL} + C_+(k, n)C_{mnL}^{lkL} & \leftrightarrow \\
C_{(m-1)(n+1)L}^{lkL} = -\frac{C_+(k, n)}{C_+(l, m-1)}C_{mnL}^{lkL} = D_{(m-1),n}C_{mnL}^{lkL} & \quad (18)
\end{aligned}$$

Here we have $L - k \leq m \leq l$ and $n = L - m$. The initial constraint is that:

$$\sum_{m=L-k}^l (C_{mnL}^{lkL})^2 = 1 = ((\dots + 1)D_{(l-1), (L-l)}^2 + 1)(C_{l(L-l)L}^{lkL})^2$$

from which we get $C_{l(L-l)L}^{lkL}$ and by repeatedly using (18) the rest of the coefficients for $M = L$ can be computed. To get the coefficients for $M < L$ use (17) with C_- .